Available online at www.sciencedirect.com
SCIENCE DIRECT
Polymer 47 (2006) 3505–3519
polymer
www.elsevier.com/locate/polymer

Comparison of fracture behavior of nylon 6 versus an amorphous polyamide toughened with maleated poly(ethylene-1-octene) elastomers

J.J. Huang, D.R. Paul *

Department of Chemical Engineering and Texas Materials Institute, The University of Texas at Austin, Austin, TX 78712, USA

Received 25 January 2006; received in revised form 10 March 2006; accepted 14 March 2006
Available online 3 April 2006

Abstract

The fracture behavior of an amorphous polyamide (Zytel 330 from DuPont), a-PA, and nylon 6 toughened by maleated poly(ethylene-1-octene) elastomers are reported. The deformation mechanisms during fracture were verified by examining an arrested crack tip and the surrounding regions using transmission electron microscopy analysis. a-PA blends show higher levels of impact strength and lower ductile–brittle transition temperatures than nylon 6 blends. Fracture toughness, characterized by both linear elastic fracture mechanics techniques in terms of the critical strain energy release rate, G_{IC}, and the essential work of fracture methodology, i.e. the limiting specific fracture energy, u_o, and the dissipative energy density, u_d, using thick (6.35 mm) samples with sharp notches, depends on ligament length, rubber content, rubber particle size and test temperature. In general, a-PA blends show larger values of u_d than do nylon 6 blends while the opposite is seen for u_o. The amorphous polyamide shows a similar critical upper limit on rubber particle size, or interparticle distance, for toughening as the semi-crystalline nylon 6; thus, it is clear that the crystal morphology around the rubber particles must not be the dominant cause of this critical size scale. The deformation mechanisms involved include cavitation of rubber particles followed by some crazing and then massive shear yielding of the matrix.

Keywords: Amorphous polyamide; Fracture behavior; Essential work of fracture

1. Introduction

We have recently explored toughening of an amorphous polyamide (Zytel 330 from DuPont) using maleated elastomers [1–3]; in part, the motivation for this work was to compare its responses with those of semi-crystalline polyamides like nylon 6 and 66 to gain insights about the role of matrix crystallinity in toughening. These studies have demonstrated that the amorphous polyamide and nylon 6 exhibit similar relationships for room temperature Izod impact strength and the ductile–brittle transition temperature (T_{db}) as rubber particle size is varied over a wide range; however; the amorphous polyamide blends have somewhat higher impact strength and lower T_{db}. The previous results were based on standard notched Izod impact testing of thin specimens (3.18 mm thick) with the standard ligament length and notch radius. It would be useful to compare the fracture behavior of blends based on the two types of polyamides under more severe plane-strain conditions, i.e. thicker (6.35 mm thick) samples with a sharp notch, and varying ligament lengths for different rubber contents and test temperatures. In addition, the deformation mechanisms of toughened blends of this amorphous polyamide are largely unexplored [4]; considerably more literature is available on how the rubber toughened semi-crystalline polyamides (e.g. nylon 6 and nylon 66) deform during fracture [5–17]. The purpose of this paper is to make these comparisons between blends based on the amorphous polyamide and nylon 6. The fracture behavior is examined as a function of rubber particle size, rubber content, ligament length and temperature via instrumented Dynatup impact tests using single-edge notched three-point bend (SEN3PB) specimens. The deformation mechanisms involved are examined in the vicinity of arrested cracks using transmission electron microscopy.

2. Background

Fracture mechanics techniques, traditionally designed for testing metallic alloys, have been employed extensively to characterize fracture behavior and to understand the deformation processes in rubber-toughened plastics [18–27]. Linear elastic fracture mechanics (LEFM) methodologies have been applied to brittle polymeric materials to measure the critical

* Corresponding author. Tel.: +1 512 471 5392; fax: +1 512 471 0542.
E-mail address: drp@che.utexas.edu (D.R. Paul).

0032-3861/$ - see front matter © 2006 Elsevier Ltd. All rights reserved.
doi:10.1016/j.polymer.2006.03.038

strain energy release rate (G_{IC}) or the critical stress intensity factor (K_{IC}). According to this model, the total fracture energy, U, is related to G_{IC} via the following equation [28,29]

$$U = U_k + G_{IC} t W \phi \quad (1)$$

where U_k is the kinetic energy of the tested specimen after fracture, G_{IC} is the critical strain energy release rate which ideally is a material parameter independent of specimen geometry, t and W are the specimen thickness and width, respectively, and the term ϕ is a function of a/w where a is the ligament length or notch depth given in the literature [29]. Plane-strain conditions are necessary for this model to apply and are ensured only if the ratio of the notch depth to the width, a/W, is less than or equal to 0.6.

While LEFM is effective for describing fracture of brittle polymers, it fails to describe fracture of ductile polymers, such as rubber-toughened blends, because these materials generally do not meet the assumptions of linear elasticity due to extensive plastic deformation surrounding the crack during fracture. Furthermore, the specimen thickness required for ensuring plain-strain conditions exceeds what can be conveniently molded. The J-integral approach [23,30], on the other hand, does not require the assumptions of linear elasticity and is regarded as more appropriate for ductile polymers. However, this methodology involves quasi-static loading and some sophisticated and labor intensive techniques for accurate crack growth measurement. Moreover, the specimen thickness required may still be greater than what can be conveniently made by injection molding.

Mai and coworkers [31–36] have developed a methodology based on Broberg's unified theory [37,38] of fracture to characterize fracture behavior of polymeric materials that is simple to implement, yet offers more detailed characterization than standard notched Izod impact tests. According to this essential work of fracture model (EWF), the total work of fracture during crack growth, W_f, can be partitioned into two components: the essential work of fracture (W_e), associated with the inner fracture process zone and the non-EWF in the outer plastic zone (W_p):

$$W_f = W_e + W_p \quad (2)$$

This model further assumes the EWF is proportional to fracture area and the non-EWF is proportional to the volume of the plastic zone:

$$w_f = w_e + \beta \ell w_p \quad (3)$$

where, w_f is the specific fracture energy, w_e is the specific essential work of fracture, β is a shape factor, ℓ is the ligament length, and w_p is the specific non-essential plastic work. The model assumes that the ligament must be fully yielded prior to crack initiation and, thus, has certain limitations on the ligament length.

Since the yielding and ligament length size criteria of the EWF method proposed by Mai and coworkers may not always be satisfied in the high speed bending configuration used in this study, a different nomenclature is employed here and in previous papers [39–42]

$$\frac{U}{A} = u_o + u_d \ell \quad (4)$$

The linear terms in the right hand side are defined as follows: u_o is the limiting specific fracture energy and u_d is the dissipative energy density. Under appropriate conditions, $u_o = w_e$ and $u_d = \beta w_p$.

The EWF approach has been used to analyze both ductile and brittle fractures. However, this approach is found to be more suitable for ductile fractures than brittle ones. The LEFM model which gives the critical strain energy release rate, on the other hand, is used to characterize only the samples failing in a brittle manner. By applying both models, the entire range of fracture behavior is quantified.

Table 1
Materials used

Designation used here	Materials (commercial designation)	Composition	Brabender torque (N m)[a]	Supplier
a-PA	Zytel 330[b]		10.7	DuPont
Nylon 6[c]	B73WP[d]		6.37[e]	Honeywell
EOR	Exact 8201	28 wt% Octene	9.5	ExxonMobil
EOR-*g*-MA-0.35%	Exxelor VA 1840	28 wt% Octene, 0.35 wt% MA	9.2	ExxonMobil
EOR-*g*-MA-1.6%	Exxelor MDEX 101-2	28 wt% Octene, 1.6 wt% MA	6.9	ExxonMobil
EOR-*g*-MA-2.5%	Exxelor MDEX 101-3	28 wt% Octene, 2.5 wt% MA	6.3	ExxonMobil

[a] Measured after 10 min at 240 °C and 60 rpm.

[b] 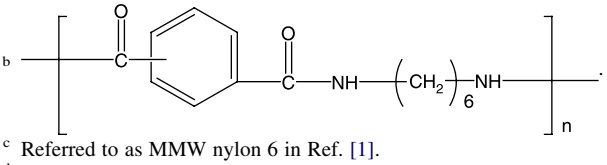

[c] Referred to as MMW nylon 6 in Ref. [1].

[d] Formerly Capron 8207F.

[e] Data from Oshinski AJ, PhD Dissertation, The University of Texas at Austin, TX, USA; 1995.

3. Experimental

Table 1 summarizes some relevant information about the materials used in this study. These materials have been used extensively in previous studies from this laboratory, and other information about these polymers is described elsewhere [2,3].

Prior to melt processing, the materials containing polyamides were dried for a minimum of 16 h in a vacuum oven at 80 °C while the neat elastomers were dried for a minimum of 16 h in a convection oven at 65 °C. All blends were made in a Haake co-rotating, intermeshing twin screw extruder (D= 3.05 cm, L/D=10) operated at 240 °C and 280 rpm. The extruded materials were pelletized and then molded into either 3.18 or 6.35 mm thick bars with an Arburg Allrounder 305-210-700 injection molding machine with the following set-up conditions: a barrel temperature of 240 °C (about 255 °C at the nozzle for molding 6.35 mm thick bars in some blends), a mold temperature of 80 °C, an injection pressure of 70 bars, and a holding pressure of 35 bars. The resulting specimens were placed into a vacuum desiccator for at least 24 h prior to testing. Since great care was taken to avoid any moisture uptake, the tested specimens may be regarded as 'dry as-molded,' typical for the literature on polyamides. Two series of blends were made; one contained a fixed 20 wt% total rubber phase but with varying proportions of the two elastomer components to control rubber particle size, and the other consisted of different total rubber contents.

The standard Izod impact tests were conducted using notched (3.18 mm thick) samples according to ASTM D256 with a TMI Impact Tester (model 43-02; 6.8 J hammer and 3.5 m/s impact velocity) equipped with a thermal chamber for cooling and heating. An instrumented Dynatup model 8200 drop tower was used for the three point blend tests using samples with dimensions of 56 mm in length, 12.7 mm in width and 6.35 mm in thickness. Testing was performed at approximately 3.4 m/s with a falling mass of 14 kg (81 J capacity at the impact velocity). Mechanical damping was applied by using a rubber pad to cover the tup and rubber bands to secure the sample ends to the testing frame; the rubber pad was made from six layers of (large size) Safeskin® latex rubber gloves. In each test, 24 samples were used with six different ligament lengths (2, 4, 5, 6, 8, 10 mm); four samples (two far end and two gate end specimens) were used for each ligament length. A sharp notch was created by tapping a fresh regular duty razor blade (0.23 mm thick) into the grove pre-made by a band saw. The testing was performed at both room temperature for all blends and at varying temperatures (−25, −10, 10, 25 °C) for selected blends. Load versus time and tup speed data were recorded; the tup speed was assumed to be a constant during impact testing, thus, allowing displacement (deflection) to be computed. The fracture energy was calculated from a numerical integration of the load–displacement data. More detailed descriptions of the set-up of the Dynatup drop tower and preparation of the samples are available elsewhere [41,43].

Blend morphology was examined using a JOEL 2010F transmission electron microscope (TEM) operated at an accelerating voltage of 200 kV. Ultra-thin sections (20 nm) were cryogenically cut perpendicular to the flow direction in a (far end) Izod bar at −45 °C with a Reichert-Jung Ultracut E microtome equipped with a diamond knife and liquid nitrogen cooling. The sections were stained in a 2% aqueous solution of phosphotungstic acid, making the polyamide phase dark in the TEM images. Apparent rubber particle size was computed from TEM photomicrographs by using a semi-automatic digital image technique based on the NIH Image® software as described previously [1–3]. Typically, at least 800 rubber particles from different views were used for analysis. The software used evaluated the area of each rubber particle, A, from which the apparent rubber particle size, d, was calculated from $d=(4A/\pi)^{1/2}$. From the distribution of rubber particle sizes, the number, weight and volume average values were computed as described previously [1–3]. For blends with a bimodal particle size distribution, the average particle size for each of the two groups was computed in addition to the global average rubber particle size.

Deformation mechanisms were assessed from TEM images taken around the tip of arrested cracks for selected blends of each of the two polyamides. The arrested cracks were generated in the 6.35 mm thick samples with a ligament length of 10 mm by adjusting the height of the hammer stop to make crack extension terminate around the mid-point of the original ligament length. This process of generating the arrested crack worked well for the blend of a-PA; however, for blends of nylon 6, the crack stopped about 2 mm away from the edge. Epoxy glue was embedded into the partially fractured samples to avoid further potential deformation during the preparation for microtoming. The observation plane was selected parallel to both the injection flow and the crack extension directions. More detailed information on preparation of the arrested cracks is given elsewhere [44,45]. Similar sectioning and staining were conducted as described above except that specimens were set at −100 °C during microtoming for viewing the microtomed thin sections in the TEM. Both bright and dark field images were taken. Photomicrographs were collected sequentially from the crack tip to the undeformed region of the specimen.

4. Izod impact strength

4.1. Effect of rubber content at room temperature

In many cases, the effect of rubber content on rubber toughening [1] has been explored by melt compounding different amounts of a given maleated elastomer with the matrix material, e.g. nylon 6, to form a binary blend. Unless the maleation level is carefully selected, the rubber particle size in such binary blends may not be optimized for toughening. Thus, blending different amounts of a single maleated elastomer with two different polyamides like nylon 6 or a-PA does not necessarily provide an accurate comparison of their toughenability. In this study, we explored the effect of the elastomer content both at room temperature and at varying temperatures while presumably keeping the rubber particle size optimized. This was done by selecting the proportion of a maleated and

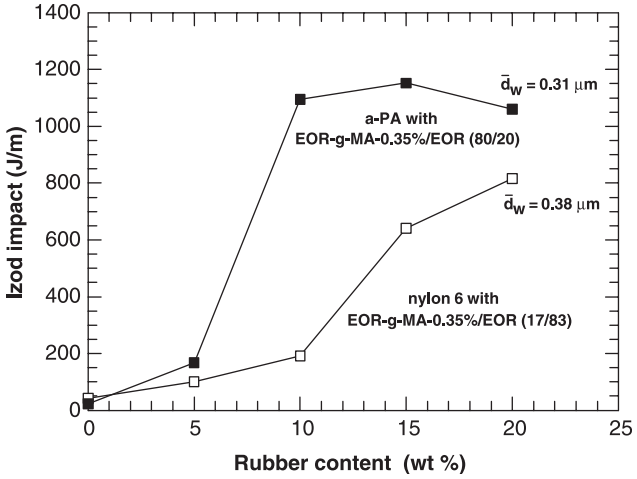

Fig. 1. Effect of rubber content on room temperature Izod impact strength of 3.18 mm thick bars with a standard notch for blends containing a mixture of EOR-*g*-MA-0.35%/EOR in the indicated proportion where the matrix material is a-PA or nylon 6.

unmaleated EOR that gave the maximum room temperature Izod impact strength for blends with nylon 6 and a-PA containing 20% total rubber. This proportion, which is different for the two polyamides, i.e. EOR-*g*-MA-0.35%/EOR = 80/20 for a-PA and 17/83 for nylon 6 as revealed from previous studies [2,3], was maintained as the total rubber content was reduced. A more refined approach would be to optimize the ratio of the rubber components at each total rubber level; however, the simple approach used should provide an adequate comparison of the two polyamides.

Fig. 1 compares the effect of total elastomer content, consisting of mixtures of EOR-*g*-MA-0.35% and EOR in the indicated proportions, on room temperature Izod impact strength (3.18 mm thick samples with a standard notch) for the two polyamides. For a-PA, the Izod values increase considerably with the rubber content as expected; super-toughness (Izod impact >800 J/m) is achieved when the rubber content is at 10% or higher while the toughness does not change very much for the rubber contents above 10%. Similarly, for nylon 6, Izod impact strength increases steadily with the total rubber content; however, super-toughness is only gained at 20% rubber content. The a-PA blends show significantly higher Izod values at the same amount of rubber than the nylon 6 blends. However, this difference becomes smaller at high rubber contents.

4.2. Effect of temperature

Fig. 2 shows the effect of temperature on Izod impact strength for the same blends of each of the polyamides as shown in Fig. 1. For a-PA, a ductile–brittle transition occurs at a certain temperature when the rubber content is at 5% or higher; this transition shifts to a lower temperature for higher rubber contents. Similar trends are observed for the nylon 6 blends. Fig. 3 compares the ductile–brittle transition temperature (T_{db}), as obtained from Fig. 2, for blends of a-PA and blends of nylon 6 as a function of rubber content. Increasing the

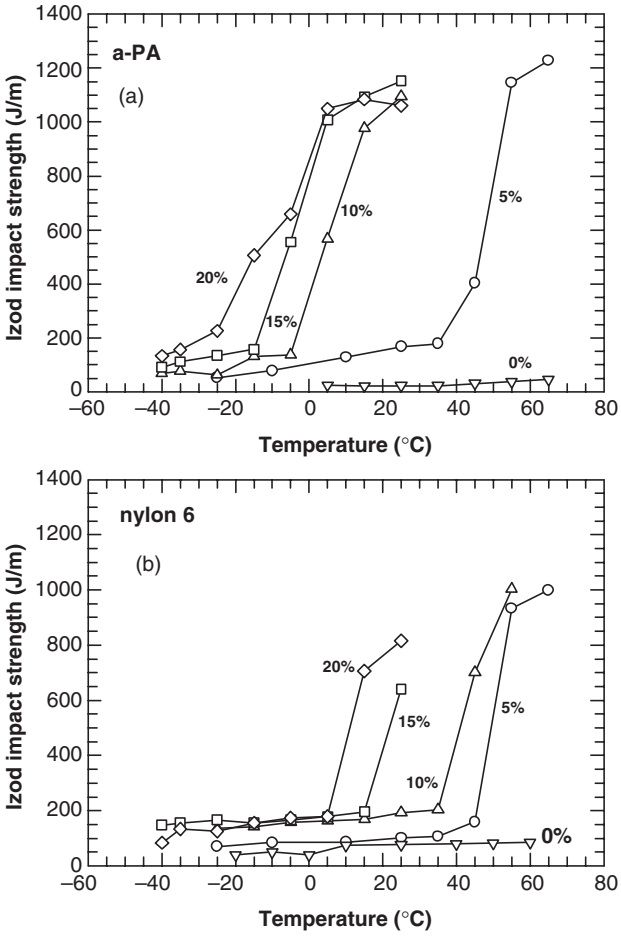

Fig. 2. Izod impact strength as a function of temperature for blends of a-PA or nylon 6 containing various rubber contents where the rubber phase consists of mixtures of EOR-*g*-MA-0.35% and EOR in a proportion of 80/20 for a-PA and 17/83 for nylon 6. Bars with a thickness of 3.18 mm were used for testing.

rubber content significantly lowers T_{db} for both polyamides; however, nylon 6 blends have a much higher ductile–brittle transition temperature, i.e. 25 °C or more, than blends of a-PA when the rubber content is at or above 5%.

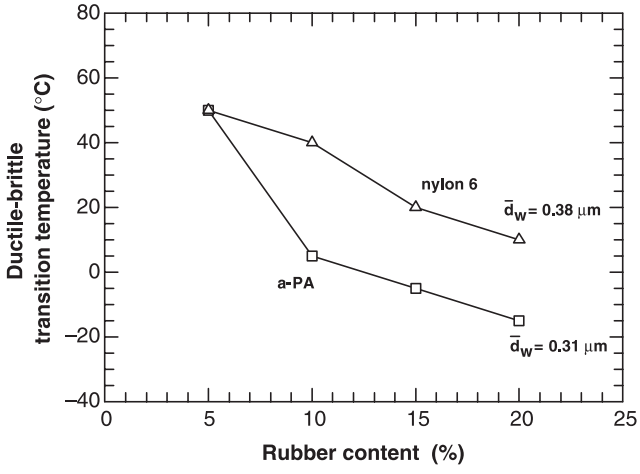

Fig. 3. Effect of rubber content on the ductile–brittle transition temperature for the blends in Fig. 2. Bars with a thickness of 3.18 mm were used for testing.

5. Dynatup fracture toughness

Our previous studies [2,3] have shown that combining any two of the four neat elastomers (Table 1) in the rubber phase in certain proportions generates a wide range of particle sizes. Under certain circumstances a bimodal size distribution appears in some blends because of immiscibility between the two elastomers when the difference in maleic anhydride (MA) level in the two rubbers exceeds a critical value of about 0.9–1.25% [2]. The occurrence of bimodality depends on the mixing ratio of the two elastomers in addition to the differences in their MA contents. In most cases, blends with a bimodal size distribution are less tough than those with a unimodal distribution in size [2].

In what follows we compare the fracture behavior of toughened blends of a-PA and of nylon 6 as a function of total rubber content and temperature using the series of blends (Figs. 1 and 2) with the optimized rubber particle size as described earlier. In addition, the fracture behavior of blends of the two polyamides at a fixed 20% total rubber content was examined as a function of particle size (unimodal distribution) over a broad range. These blends were purposely chosen to span the range of particle sizes from the lower limit to the upper limit. In some cases, the far and gate ends of the Izod bars showed significantly different fracture behavior. Finally, two nylon 6 blends were formulated with unimodal particle size distributions that have about the same global average particle sizes as two blends having a bimodal particle size distribution. The difference in fracture behavior between these two types of blends is demonstrated. In all cases, the fracture behavior was examined using single edge notched three-point bend specimens (thickness = 6.35 mm) with a sharp notch.

5.1. Effect of rubber content at room temperature

Fig. 4 shows the total fracture energy per unit area, *U/A*, as a function of ligament length for blends of each of the two polyamides containing various rubber contents where the rubber phase consists of a mixture of EOR-*g*-MA-0.35% and EOR in a proportion of 80/20 for a-PA and 17/83 for nylon 6. Blends of a-PA with 15 and 20% of total rubber show ductile fracture and *U/A* increases nearly linearly with the ligament length; the values of *U/A* are greater for the blend containing 20% than for the blend containing 15%. The blends of a-PA with 0, 5, and 10% rubber, show brittle fracture and *U/A* is essentially independent of the ligament length with values in the order, 10% > 5% > 0%, as might be expected. Blends of nylon 6 with 20% total rubber show ductile fracture and *U/A* increases with the ligament length; however, the values of *U/A* and the slope of this line are both smaller than for the corresponding a-PA blend. The data for the nylon 6 blend show considerable more scatter than that for a-PA. For the blend with 15% rubber, specimens show ductile failure when the ligament length is less than 5.2 mm but brittle failure at longer ligament lengths. Similar ductile-to-brittle transitions have been seen in other rubber toughened systems and explained in terms of the relative stress levels required for yielding versus crack

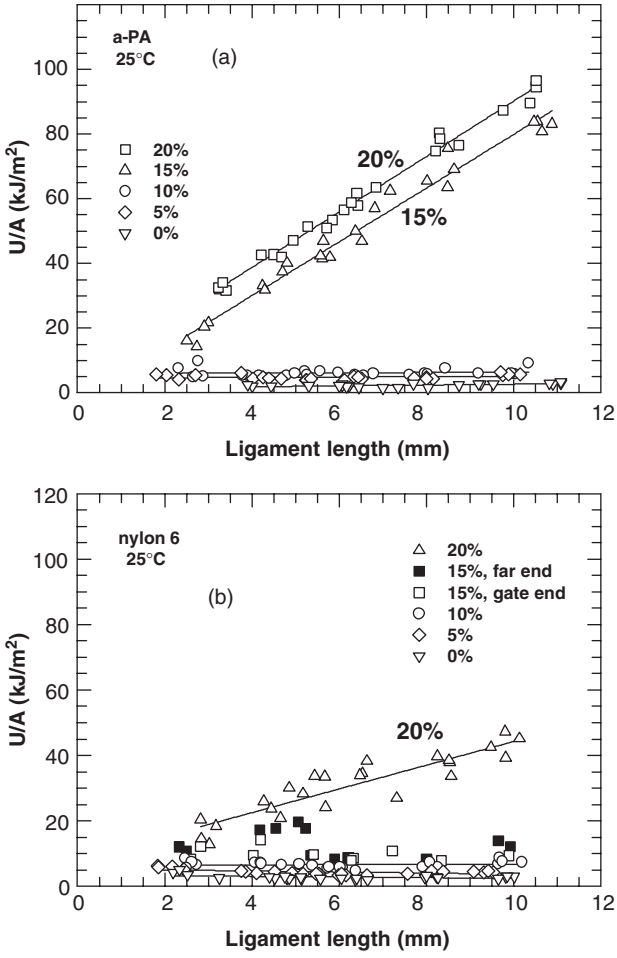

Fig. 4. Total fracture energy per unit area, *U/A*, versus ligament length for thick specimens (6.35 mm) with a sharp notch at room temperature for a series of blends of a-PA and for nylon 6 with various rubber contents based on mixtures of EOR-*g*-MA-0.35%/EOR in a proportion of 80/20 for a-PA and 17/83 for nylon 6.

propagation [40,46]. The gate end specimens failed in a brittle fashion for all ligament lengths. The gate and far end differences are due to differences in rubber particle shape along the bar [1]. For the blends of nylon 6 with 0, 5, and 10% of total rubber, *U/A* is essentially independent of ligament length with the values in the order of 10% > 5% > 0%.

Table 2 shows the effect of rubber content on the intercept of the *U/A* versus ligament length curve, i.e. the limiting specific fracture energy, u_o, of the blends containing various rubber contents. Clearly, u_o increases with rubber content as might be expected. Fig. 5 shows how the slope or the dissipative energy density, u_d, of plots of *U/A* versus ligament length (obtained by linear regression analysis of the data in Fig. 4) depends on rubber content for the a-PA and nylon 6 blends. This slope, or u_d, on the other hand, is essentially zero up to 10% and then increases considerably; the a-PA blends show considerably higher values than the nylon 6 blends. The transition from brittle to ductile failure takes place as the rubber content exceeds 10%. In essence, u_d is a measure of the extent of plastic deformation in the region extending beyond the crack and correlates with the size of the stress whitened zone. These

Table 2
Effect of rubber content on the limiting specific fracture energy, u_o, of blends of a-PA and blends of nylon 6

Matrix	Rubber content	u_o (kJ/m^2)
a-PA	0% EOR-*g*-MA-0.35%/EOR (80/20)	1.35±0.34
	5%	4.54±0.38
	10%	5.92±0.69
	15%	6.31±2.14
	20%	6.95±1.22
Nylon 6	0% EOR-*g*-MA-0.35%/EOR (17/83)	2.26±0.24
	5%	4.39±0.78
	10%	6.48±0.55
	15%	7.21±2.8
	20%	8.0±2.40

observations are consistent with the higher Izod impact strength for a-PA blends than for nylon 6 blends as seen in Fig. 1.

5.2. Effect of rubber particle size at room temperature

5.2.1. Blends with a unimodal size distribution

Fig. 6 shows how *U*/*A* depends on ligament length for blends of the two types of polyamides containing fixed total rubber content of 20% as the rubber particle size is varied by changing the maleation level in the rubber phase by blending; in every case, the particle size distribution is unimodal. For a-PA, blends with $\bar{d}_w = 0.14$ and 0.31 μm show ductile fracture for all ligament lengths; the *U*/*A* versus ligament line has a larger slope for the blend with $\bar{d}_w =$ 0.31 μm than for the blend with $\bar{d}_w = 0.14$ μm. However, brittle failure occurs for blends having larger particle sizes than 0.5 μm. The blend with $\bar{d}_w = 0.5$ μm shows a ductile–brittle transition in ligament length at about 7.5 mm. Similarly, for nylon 6, blends with $\bar{d}_w$ of 0.38 μm or smaller shows ductile failure while brittle failure is seen for blends with bigger particle sizes of 1.19 or 2.70 μm.

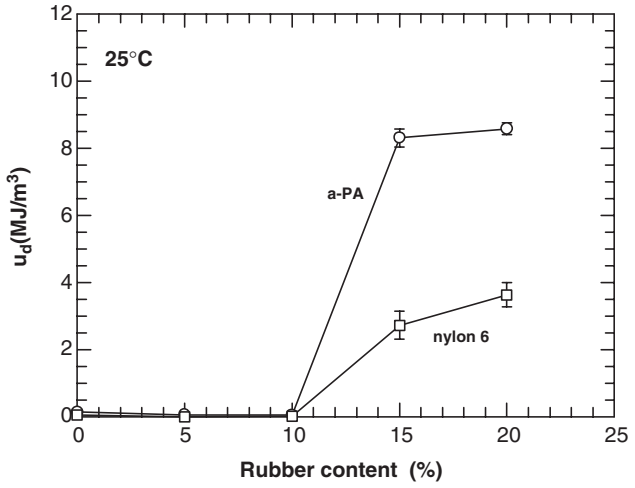

Fig. 5. Effect of rubber content on the dissipative energy density, u_d, at room temperature for thick (6.35 mm) specimens with sharp notches formed from the series of blends shown in Fig. 4.

Fig. 7 shows the effect of rubber particle size on the intercept, or u_o and slope, u_d, obtained from Fig. 6 via linear regression. For a-PA, u_o increases steadily with rubber particle size and reaches a maximum when the particle size is about 0.80 μm and then decreases rapidly. Similarly, for nylon 6, u_o increases considerably with rubber particle size and is at a maximum at a particle size of about 0.2 μm, and then decreases gradually. Nylon 6 blends have larger u_o values than a-PA blends in the particle size range from about 0.15 to 0.8 μm; however, u_o is about the same for blends of the two polyamides for particle sizes above 0.8 μm. The u_d values for blends of a-PA increase with rubber particle size and has a maximum at about 0.3 μm, then decreases dramatically. When the particle size is above about 0.75 μm, u_d is essentially zero. For nylon 6, however, u_d increases rather gradually with particle size and appears to have a broad plateau from about 0.2 to 0.9 μm, and then goes to zero for larger particle sizes. a-PA blends show much larger u_d values than blends of nylon 6 in the particle size range from 0.15 to 0.5 μm. This difference in u_d, or the size of plastic deformation zone, explains why blends

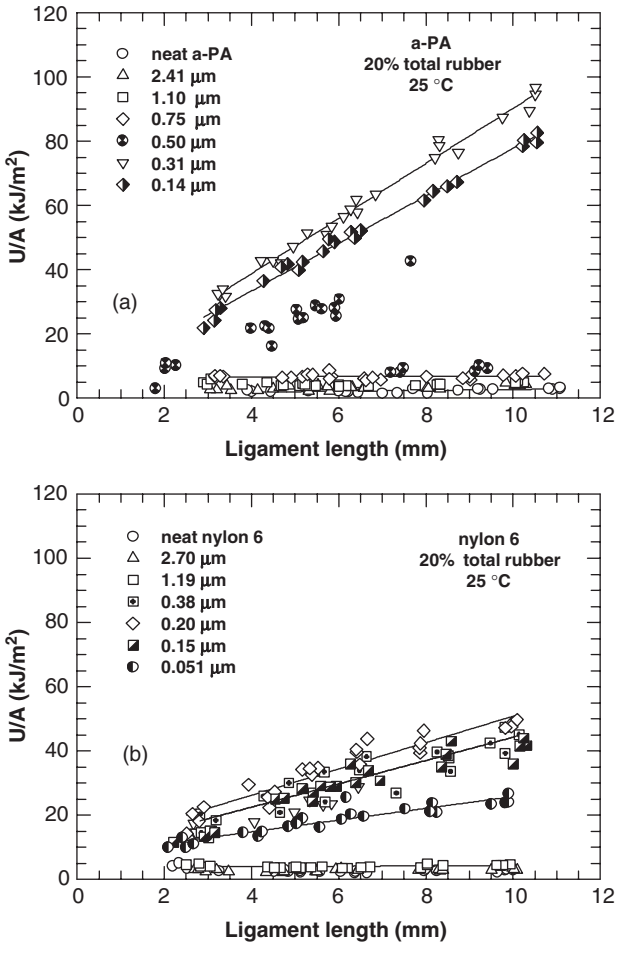

Fig. 6. Total fracture energy per unit area, *U*/*A*, versus ligament length for blends of a-PA or nylon 6 with a fixed 20% of rubber where the rubber phase consists of either mixtures of EOR-*g*-MA-0.35% and EOR in varying proportions or neat EOR-*g*-MA-1.6% to vary rubber particle size. Testing was performed at room temperature using thick specimens (6.35 mm) with sharp notches.

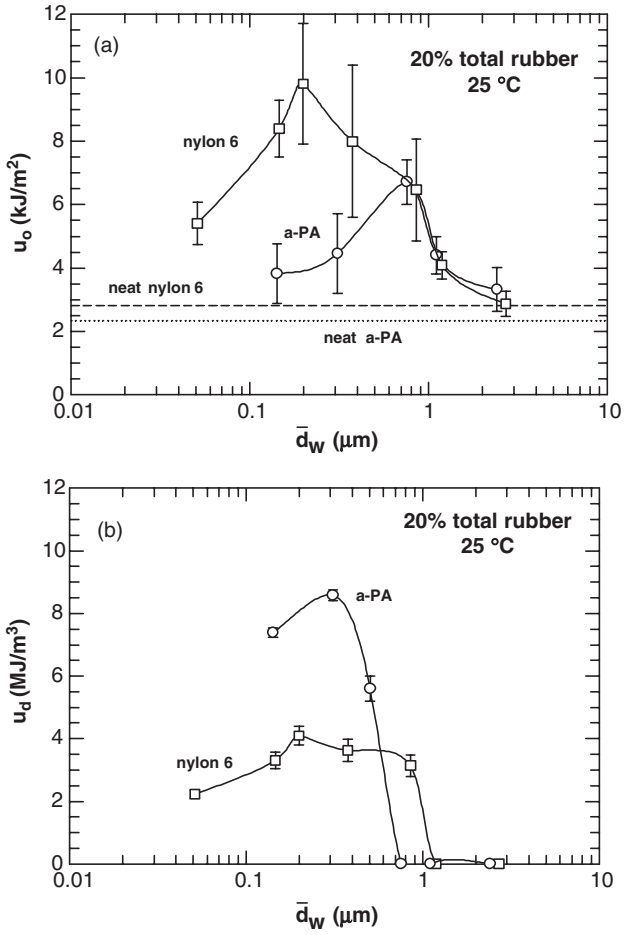

Fig. 7. Effect of rubber particle size on the limiting specific fracture energy, u_o, part; (a), and the dissipative energy density, u_d, part; (b), for the blends of a-PA or nylon 6 shown in Fig. 6. Thick samples (6.35 mm) with sharp notches were used for testing at room temperature.

of a-PA show larger Izod impact strength in previous studies than nylon 6 blends for the rubber particle size within the optimum range. The trend of u_d with particle size shown here is rather similar to the trend for Izod impact strength shown previously; thus, plots of u_d versus rubber particle size provide another way to define the upper and lower critical particle size limits for toughening. Interestingly, the essential work of fracture, or u_o, and the non-essential work of fracture, or u_d, show similar trends with particle size. It would appear that the energy to form the crack and the energy dissipated in the stress whitened zone are related.

5.2.2. Far end versus gate end differences for nylon 6 blends

For well-toughened polyamides, there is generally a negligible difference in impact properties between the two ends of an injection molded bar; however, when the blend is near any type of ductile–brittle transition, such as those seen by varying temperature, rubber content, rubber particle size or ligament length, dramatic differences in impact strength may be seen along the length of the bar [40,47,48] owing to small differences in morphology caused by the flow during mold filling. Previous work on a-PA with maleated

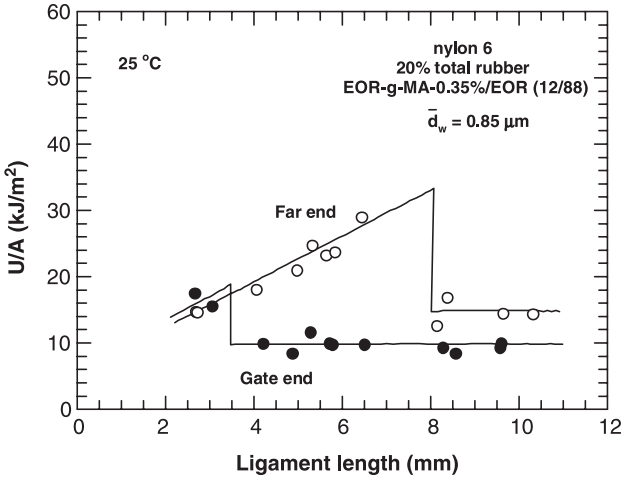

Fig. 8. Total fracture energy per unit area versus ligament length for a blend of nylon 6 with 20% total rubber where the rubber phase is composed of a mixture of EOR-*g*-MA-0.35% with EOR in a proportion of 12/88 showing differences in far end and gate end specimens. Testing was performed at room temperature using thick (6.35 mm) specimens with sharp notches.

and non-maleated SEBS [1] demonstrated that the far end samples were much tougher than the gate end specimens in certain blends; this difference in toughness was attributed to the fact that the rubber particles in the gate end are highly elongated relative to the case for the far end due to the flow deformation. In this study, 24 samples were used for each blend where half of them are far end specimens and the remaining half are gate end ones. In most cases, it is not necessary to distinguish between the two ends; however, when there is a significant difference in fracture energy between the two ends, the two groups of specimens are averaged and presented separately. Fig. 8 compares the relationship of *U/A* versus ligament length between far end and gate end samples for a blend of nylon 6 with average particle size of 0.85 μm at 20% total rubber. Clearly, both far end and gate end samples exhibit a ductile–brittle transition in ligament length; this transition occurs at a ligament length of 6.5–8.0 mm for the far end samples and at 3.0–3.5 mm for the gate end specimens.

5.2.3. Effect of rubber particle size distribution on toughness of nylon 6 blends

Two blends of nylon 6 with 20% total rubber were prepared to have bimodal size distributions with about the same global weight average rubber particle sizes as two blends of nylon 6 having a unimodal size distribution (Fig. 6). For the blends exhibiting bimodality, it was demonstrated in previous studies that the global average size was inappropriate for correlating Izod impact strength and the ductile–brittle transition temperature [2,3]. In this case, a suitable approach seems to be to compute an average size for each of the two populations and use these values to correlate Izod impact strength, i.e. two sizes for one Izod value. This approach has been shown to be more coherent for locating the lower or upper critical size limit for toughening. It would be of interest to examine any differences in fracture toughness between blends with unimodal versus bimodal size distributions when the global

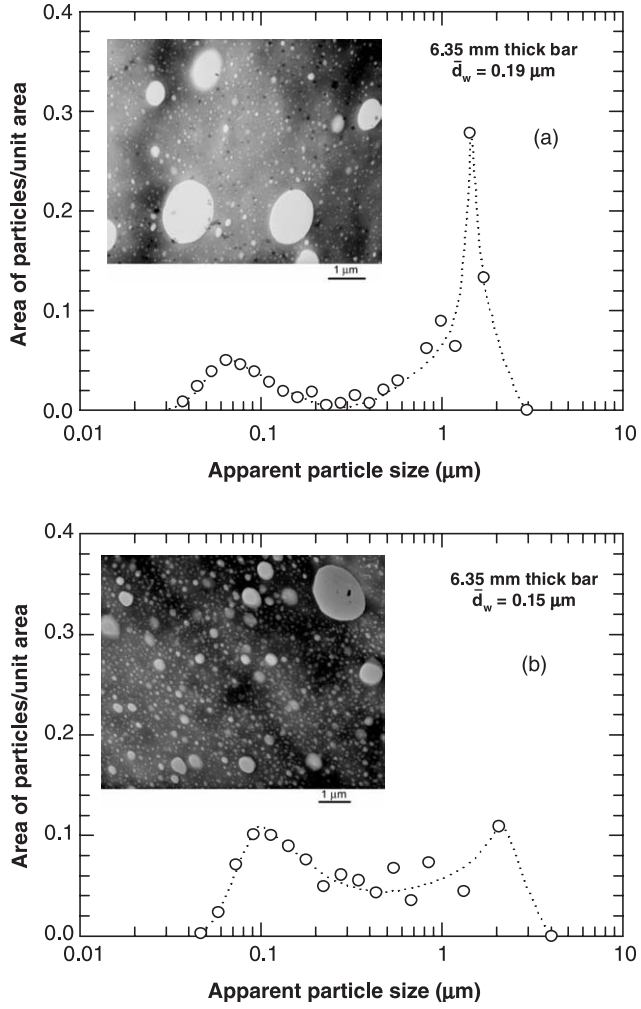

Fig. 9. TEM photomicrographs and size distributions for two nylon 6 blends containing a mixture of EOR-*g*-MA-2.5%/EOR (18/82); (a) and a mixture of EOR-*g*-MA-1.6%/EOR (28/72); (b) thick samples (6.35 mm) were used. Polyamide phase was stained dark with phosphotungstic acid.

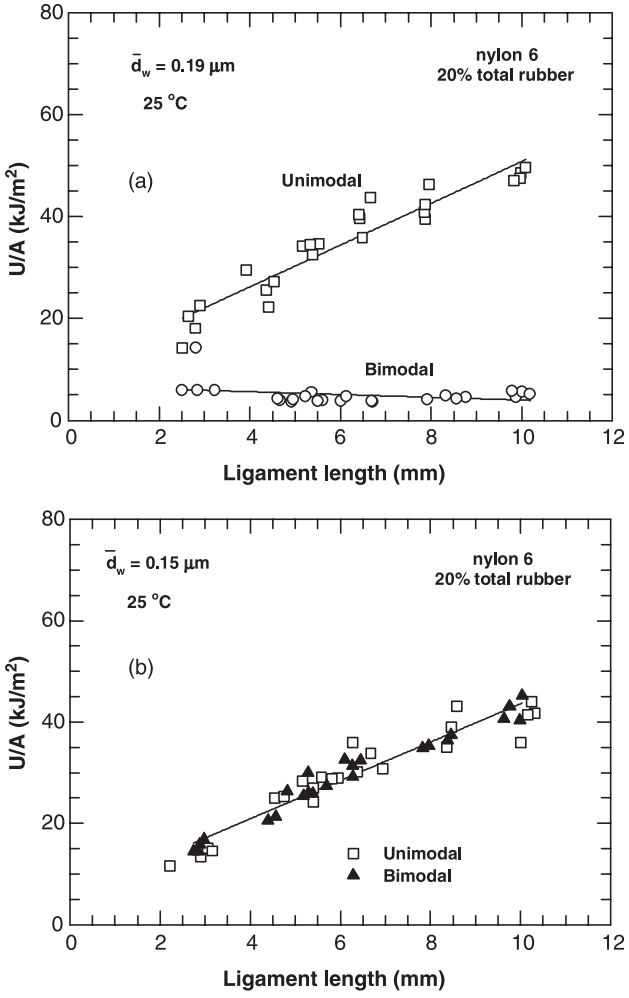

Fig. 10. Total fracture energy per unit area versus ligament length for two sets of blends of nylon 6 with 20% total rubber with the global average rubber particle sizes shown. In each case, one blend has a unimodal size distribution and the other blend has a bimodal size distribution. For the pair with a global particle size of 0.19 μm (a), the blend with the unimodal size distribution contains a mixture of EOR-*g*-MA-0.35%/EOR (40/60) and the blend with the bimodal size distribution consists of a mixture of EOR-*g*-MA-2.5%/EOR (18/82). For the pair with a global particle size of 0.15 μm (b), the blend with a unimodal size distribution contains a mixture of EOR-*g*-MA-0.35%/EOR (60/40) and the blend with a bimodal size distribution consists of a mixture of EOR-*g*-MA-1.6%/EOR (28/72).

average particle size is fixed. Fig. 9 shows TEM photomicrographs and particle size distributions for nylon 6 blends based on mixtures of EOR-*g*-MA-2.5%/EOR in a proportion of 18/82 (a) and mixtures of EOR-*g*-MA-1.6%/EOR in a proportion of 28/72 (b) in the (20%) rubber phase, respectively, examined in 6.35 mm thick bars. Clearly, a bimodal distribution of particle size is seen.

Fig. 10 compares *U*/*A* versus ligament length for the two pairs of nylon 6 blends where within each pair one has a unimodal particle size distribution and the other a bimodal size distribution, but the two distributions have the same global average rubber particle size. For the pair having global $\bar{d}_w = 0.19$ μm, the blend with a bimodal size distribution shows brittle fracture while ductile failure is seen for the blend with a unimodal distribution. For the pair with a global weight average particle size of 0.15 μm, however, both blends exhibit ductile fracture with about the same *U*/*A* value. These differences may be understood in terms of how rubber particle size affects Izod impact strength shown in previous studies [1–3]. For the bimodal blend having a global average size of 0.19 μm, the $\bar{d}_w$ for the smaller population (0.078 μm) lies below the lower particle size limit for effective toughening while the $\bar{d}_w$ for the larger population (0.71 μm) lies just above the upper limit for effective toughening. As a result, for this bimodal blend, the two populations separately would not lead to toughness so brittle failure of the composite distribution might be expected. On the other hand, for the bimodal blend with a global average size of 0.15 μm, the average sizes of the smaller population (0.092 μm) and the larger population (0.51 μm) both fall within the range of optimum size for toughening. It is reasonable that a blend having two populations of particles that separately would lead to toughness might also be tough. Thus, the rubber particle size for each

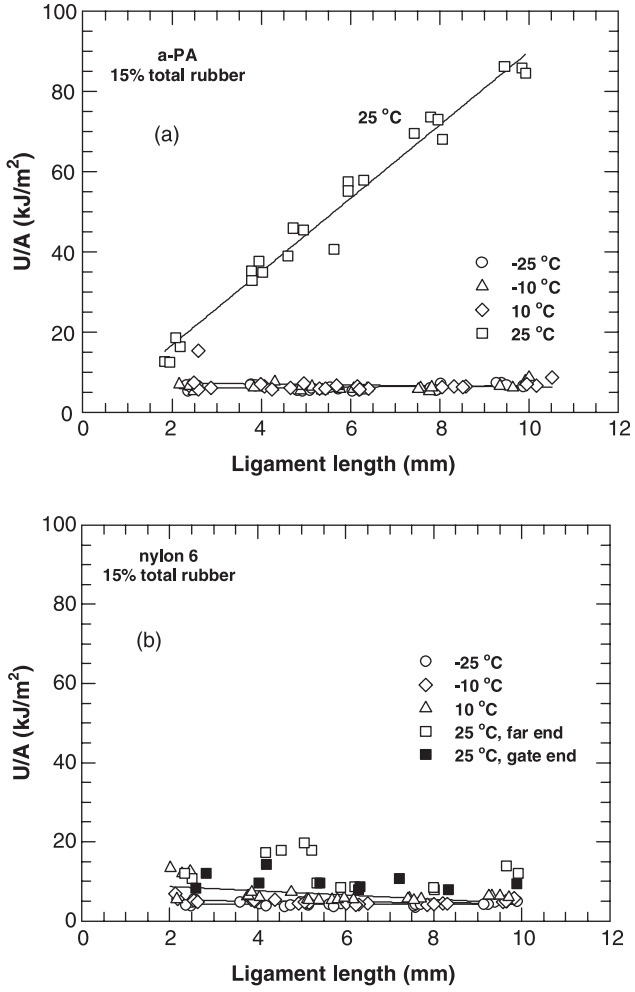

Fig. 11. Total fracture energy per unit area versus ligament length at different temperatures for the blend of each of the two polyamides containing 15% total rubber comprising a mixture of EOR-*g*-MA-0.35%/EOR in a proportion of 80/20 for a-PA and 17/83 for nylon 6. Thick (6.35 mm) specimens with sharp notches were used for testing.

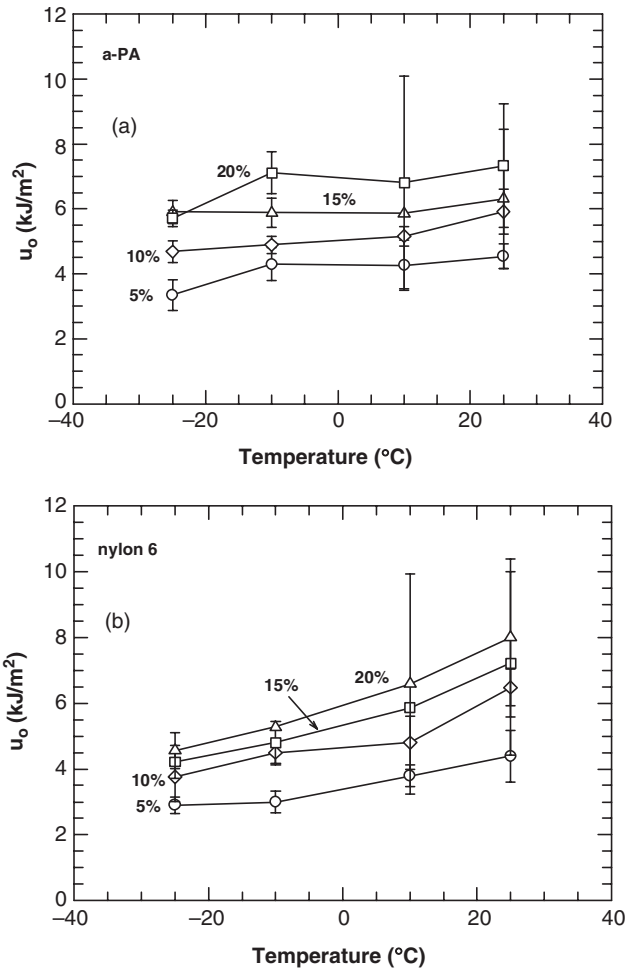

Fig. 12. Limiting specific fracture energy, u_o, as a function of temperature for the series of blends specified in Fig. 4. Thick specimens (6.35 mm) with sharp notches were used for testing.

population, rather than the global average, is the key to elucidating the fracture behavior.

5.3. Effect of temperature

The fracture toughness results discussed to this point were based on room temperature measurements. In this sub-section, the effect of temperature on fracture behavior will be explored for blends where the total rubber content is varied but the rubber phase consists of a mixture of EOR-*g*-MA-0.35%/EOR with a ratio of 80/20 for a-PA and 17/83 for nylon 6. Fig. 11 shows how fracture energy per unit area, *U*/*A*, responds to ligament length at varying temperatures for blends of a-PA and of nylon 6 containing 15% of total rubber. For a-PA, ductile fracture is seen at room temperature while brittle failure occurs at all other temperatures (10, −10, −25 °C) with about the same value of *U*/*A*. For nylon 6, however, the blend fails in a brittle fashion at temperatures other than 25 °C with larger values of *U*/*A* for higher temperatures; far and gate end differences are seen at room temperature as described earlier.

Fig. 12 shows the effect of temperature on the limiting specific fracture energy, u_o, for the blends of each of the polyamides containing various rubber contents. In general, u_o increases with temperature and with rubber content for blends based on the two polyamides. It appears that the temperature dependence may be greater or more well-defined for nylon 6 than for a-PA. There is a large standard deviation in these values in some cases; this must be remembered when attempting to interpret these trends too closely. Fig. 13 shows the dissipative energy density, u_d, as a function of temperature for blends containing various rubber contents where the matrix material is either a-PA or nylon 6. For a-PA, blends containing 5 or 10% of total rubber essentially exhibit brittle failure at all temperatures tested, i.e. u_d is very small or zero. However, blends containing 15% or 20% rubber shows ductile–brittle transitions as the temperature increases with the values of u_d increasing with temperature thereafter. For nylon 6, similar trends are seen except that the values of u_d are much smaller than that for the corresponding a-PA blends at the same temperature.

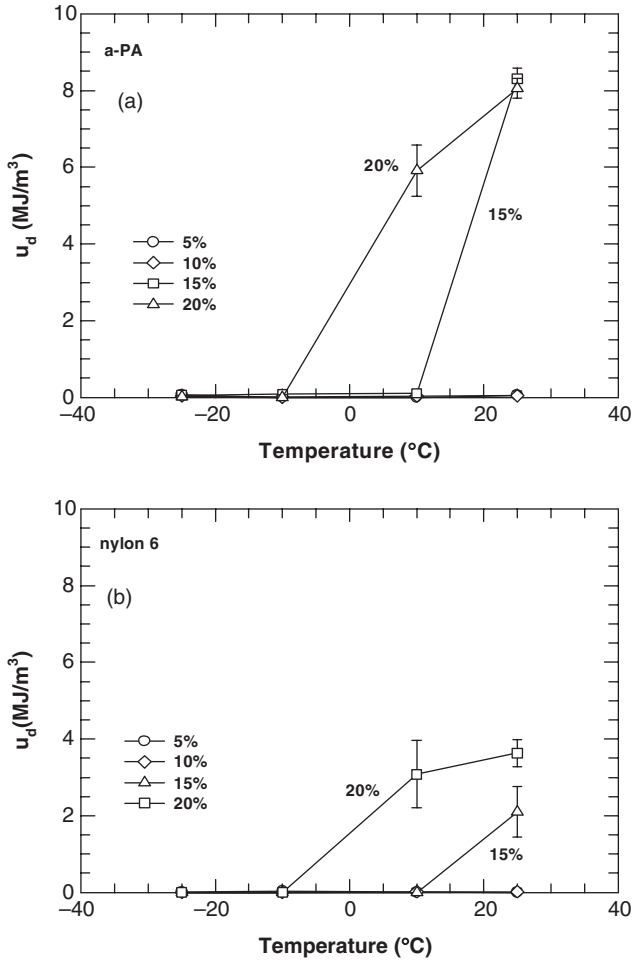

Fig. 13. Dissipative energy density, u_d, as a function of temperature for the series of blends used in Fig. 4. Thick specimens (6.35 mm) with sharp notches were used for testing.

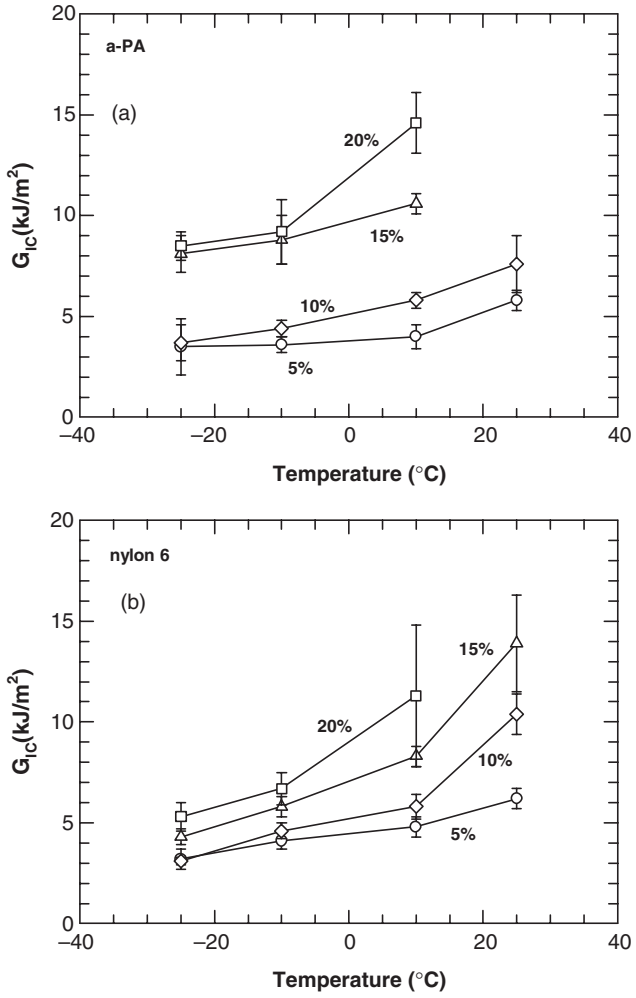

Fig. 14. Effect of temperature on the critical strain energy release rate, G_{IC}, for the series of blends used in Fig 4. Thick specimens (6.35 mm) with sharp notches were used for testing.

5.4. Critical strain energy release rate

5.4.1. Effect of temperature

Linear elastic fracture mechanics (LEFM) techniques may be used to quantify the fracture behavior of specimens exhibiting brittle failure in terms of the critical strain energy release rate, G_{IC}. The LEFM techniques employ the same experimental procedures, as described in the experimental section, as the essential work of fracture methodology for making and testing samples; however, there is a difference in the data analysis. For the LEFM approach, instead of using the total fracture energy, as in the case of the EWF method, the fracture energy at peak load ($U_{peakload}$) is obtained manually by numerical integration of the load versus displacement curve; this energy at peak load is plotted versus the term $tW\phi$, see Eq. (1), to obtain the slope, i.e. G_{IC}, by linear regression. In this study, the LEFM approach is employed for the two series of blends that fail in a brittle fashion for each of the two polyamides in order to explore the effects of temperature and rubber particle size on fracture behavior.

Fig. 14 shows the critical strain energy release rate, G_{IC}, obtained from the slope of $U_{peakload}$ versus $tW\phi$, as a function of temperature for the blends of each of the two polyamides containing various rubber contents. For a-PA, G_{IC} is seen to increase gradually with temperature and higher rubber content leading to larger values of G_{IC}. In other words, even though the fracture is brittle, the energy dissipated increased with increasing temperature and rubber content as might be expected. For nylon 6, the values of G_{IC} are generally lower but similar trends are seen; the increase in G_{IC} seems more significant at temperatures higher than 10 °C. Similar effects of temperature on G_{IC} have been reported for the nylon 6/ABS system [42].

5.4.2. Effect of rubber particle size at room temperature

The effect of rubber particle size on the critical strain energy release rate, G_{IC}, at room temperature is shown in Table 3 for some of the blends based on each of the two polyamides with a fixed 20% of total rubber where the rubber phase contains a mixture of EOR-*g*-MA-0.35% with EOR in various proportions. For both polyamides, G_{IC} is observed to decrease with particle size; however, nylon 6 blends show a higher value of G_{IC} than do a-PA blends in all cases examined. The difference

Table 3
Effect of rubber particle size on the critical strain energy release rate, G_{IC}, of blends of a-PA and blends of nylon 6

Matrix (80%)	Rubber phase (20%)	$\bar{d}_w$ (μm)	$\bar{d}_w/\bar{d}_n$	$\bar{d}_v/\bar{d}_n$	G_{IC} (kJ/m^2)
a-PA	EOR-*g*-MA-0.35%/EOR = 25/75	0.75	1.59	2.94	5.90±0.9
	10/90	1.10	1.56	2.51	4.40±0.2
	0/100	2.41	1.26	1.78	2.50±0.3
Nylon 6	EOR-*g*-MA-0.35%/EOR = 12/88	0.85	1.64	3.07	9.80±0.6
	6/94	1.19	1.90	3.55	4.80±0.3
	0/100	2.70	1.37	1.72	2.70±0.3

becomes negligible for particle sizes above 1 μm. Similar trends have been observed for nylon 6 blends with other elastomers [40,43].

6. Deformation mechanisms

For semi-ductile polymers, the triaxial stress field ahead of a crack tip can preclude shear yielding and cause brittle failure [49]. However, for rubber-toughened semi-ductile polymers, cavitation of the rubber particles ahead of the crack may release the triaxial stresses which in turn allows shear yielding of the matrix material to occur, i.e. ductile fracture [49]. The purpose here is to verify that this mechanism applies for a-PA blends as is known to be the case for nylon 6 blends. This is done at room temperature by examining an arrested crack and the surrounding regions, formed during testing of 6.35 mm thick specimens with sharp notches, using TEM analysis of a blend of a-PA containing 20% of total rubber where the rubber phase consists of a mixture of EOR-*g*-MA-0.35%/EOR (80/20) and a nylon 6 blend with 20% of total rubber composed of a mixture of EOR-*g*-MA-0.35%/EOR (40/60) in the rubber phase; each of the blends exhibits the highest toughness for the two polyamides (Fig. 6). Both TEM bright and dark field images were used for showing the morphology; the former forms an image using the direct electron beam while the latter does so using the scattered electron beam [50]. Bright field images are the opposite of dark field images in terms of the intensity observed at a given position. Dark field images are particularly useful for verifying cavitation of rubber particles since cavities will appear darker than non-cavitated particles. Figs. 15 and 16 show TEM photomicrographs at the crack tip and the region ahead of the tip for the two polyamide blends. For both materials, the rubber particles around the crack tip (Figs. 15(a) and 16(a)) exhibit extensive deformation consistent with being sheared; consequently, the matrix polyamide between the deformed rubber particles must have undergone shear yielding. Images from slightly ahead of the crack tip (about 18 μm for a-PA, Fig. 15(b), and about 30 μm for nylon 6, Fig. 16(b)) also show evidence of shear deformation. Images from further away from the tip, about 0.8 mm away for a-PA and about 0.5 mm away for nylon 6 (see Figs. 15(c) and 16(c)) but still inside the stress-whitened zone (SWZ), show rows of cavitated rubber particles with what appears to be shear-yielded polyamide ligaments between them. Cavitation of the rubber particles is verified by viewing the same area in the dark field mode, see Figs. 15(d) and 16(d); the holes inside the particles appear very dark. Such rows of cavitated rubber particles seem to involve only the larger particles rather than the smaller ones; larger particles cavitate more easily than smaller ones [16]. For rubber toughened polyamides, Lazzeri and Bucknall have reported similar lines of cavitated rubber particles separated by shear yielded polyamide ligaments and referred to these features as 'dilational bands' [51]. Similar dilational bands have been observed in nylon 6 blends based on maleated ethylene/propylene elastomers with or without glass fibers [43,45]. Sue et al. have also reported similar arrays of cavitated rubber particles in rubber-toughened epoxy matrices and called them 'croids' [52–54]. In the region about 1.1 mm outside the SWZ, images for both polyamides show extensive cavitation of rubber particles, see Figs. 15(e) and 16(e), not involving dilational bands; again the very small particles do not seem to cavitate. Cavitation is verified by dark field images of the same area in each polyamide as seen in Figs. 15(f) and 16(f); black spots inside some of the rubber particles reflect holes. The a-PA blend seems to have less extensive cavitation than the nylon 6 blend. Interestingly in about the same region, multiple crazing is observed for a-PA, see Fig. 15(g), while single crazes are seen in between rubber particles for nylon 6, see Fig. 16(g). Crazing is further verified by dark field images shown in Figs. 15(h) and 16(h) of the same position. The crazes show typical characteristics, i.e. many fibrils with interconnected voids over a given length. The crazing is believed to be associated with localized stress fields favoring craze formation. The a-PA blend seems to show more crazing than the nylon 6 blend; however, for both polyamides, the crazing is observed only in selected regions ahead of the SWZ and is not seen pervasively through the entire region. Based on this cursory examination, it is believed that rubber particle cavitation followed by some crazing and then massive shear yielding of the matrix accounts for most of the energy dissipation [8,17]. It would be interesting to use other techniques, e.g. scattering methods, that can apportion the relative extent of deformation to the different mechanisms [55–59].

There is an extensive literature on the toughening and plastic deformation of nylon 6 and nylon 66 [9,11,14,60–67], but there is a very limited literature on such behavior for this amorphous polyamide [1–4,68,69]. To our knowledge, no evidence has been reported on crazing of a-PA materials. It would be very useful to conduct follow on studies designed to be sure that the crazing we report here is not the result of some artifact, such as specimen preparation like microtoming, and to better define the circumstances where it does occur and its relative role in the toughening mechanism.

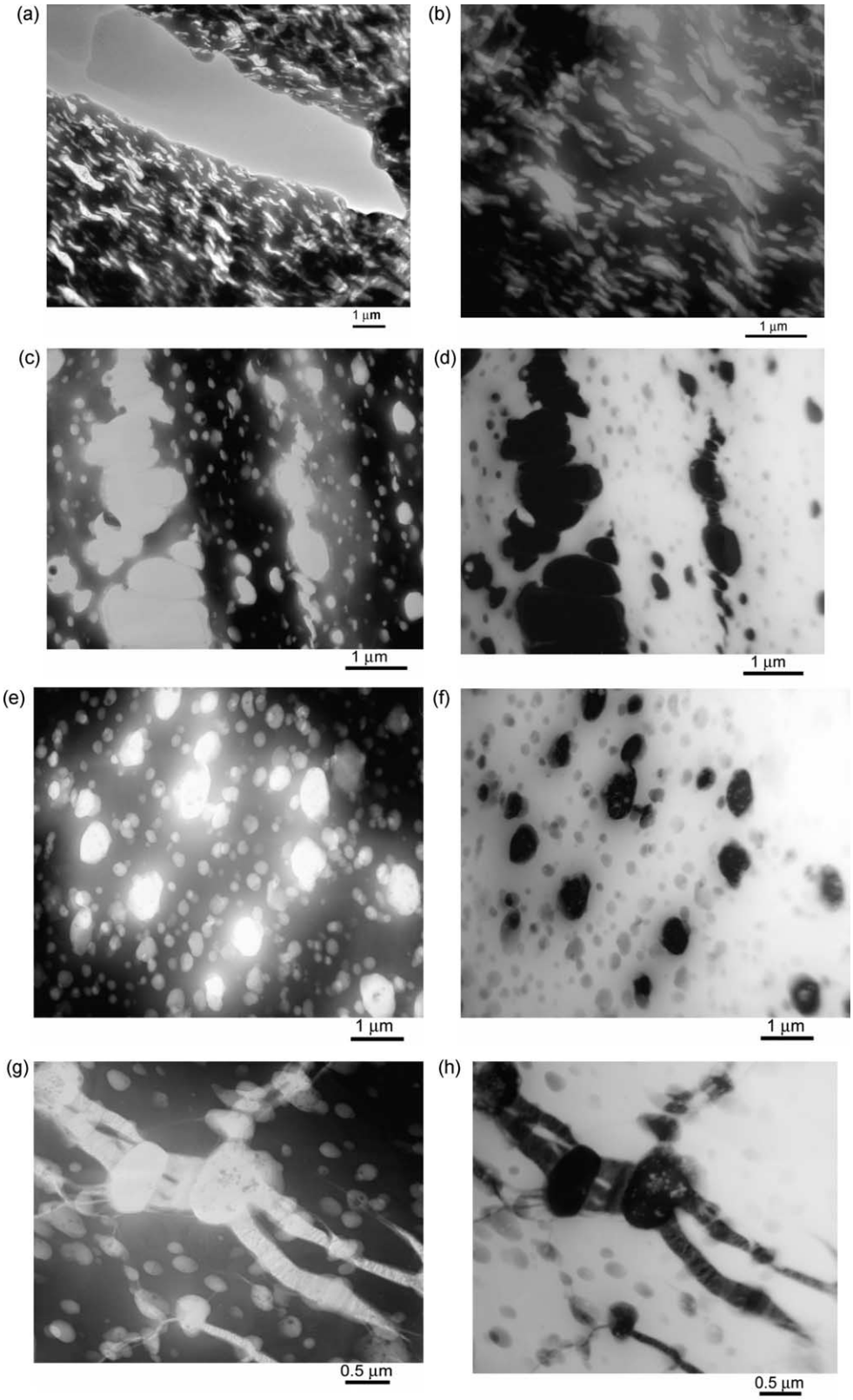

Fig. 15. TEM photomicrographs showing the morphology in the vicinity of an arrested crack tip in a 6.35 mm thick specimen with a sharp notch of a blend of a-PA containing 20 wt% of a mixture of EOR-*g*-MA-0.35%/EOR in a proportion of 80/20 in the rubber phase; (a) bright field image of the crack tip; (b) bright field image of about 18 μm ahead of the crack tip; (c) bright field image about 0.8 mm ahead of the crack tip but still inside the stress whitened zone (SWZ); (d) dark field image of (c); (e) bright field image about 1.1 mm ahead of the SWZ (about 4.6 mm away from the crack tip); (f) dark field image of (e); (g) bright field image from about the same position as (e); and (h) dark field image of (g).

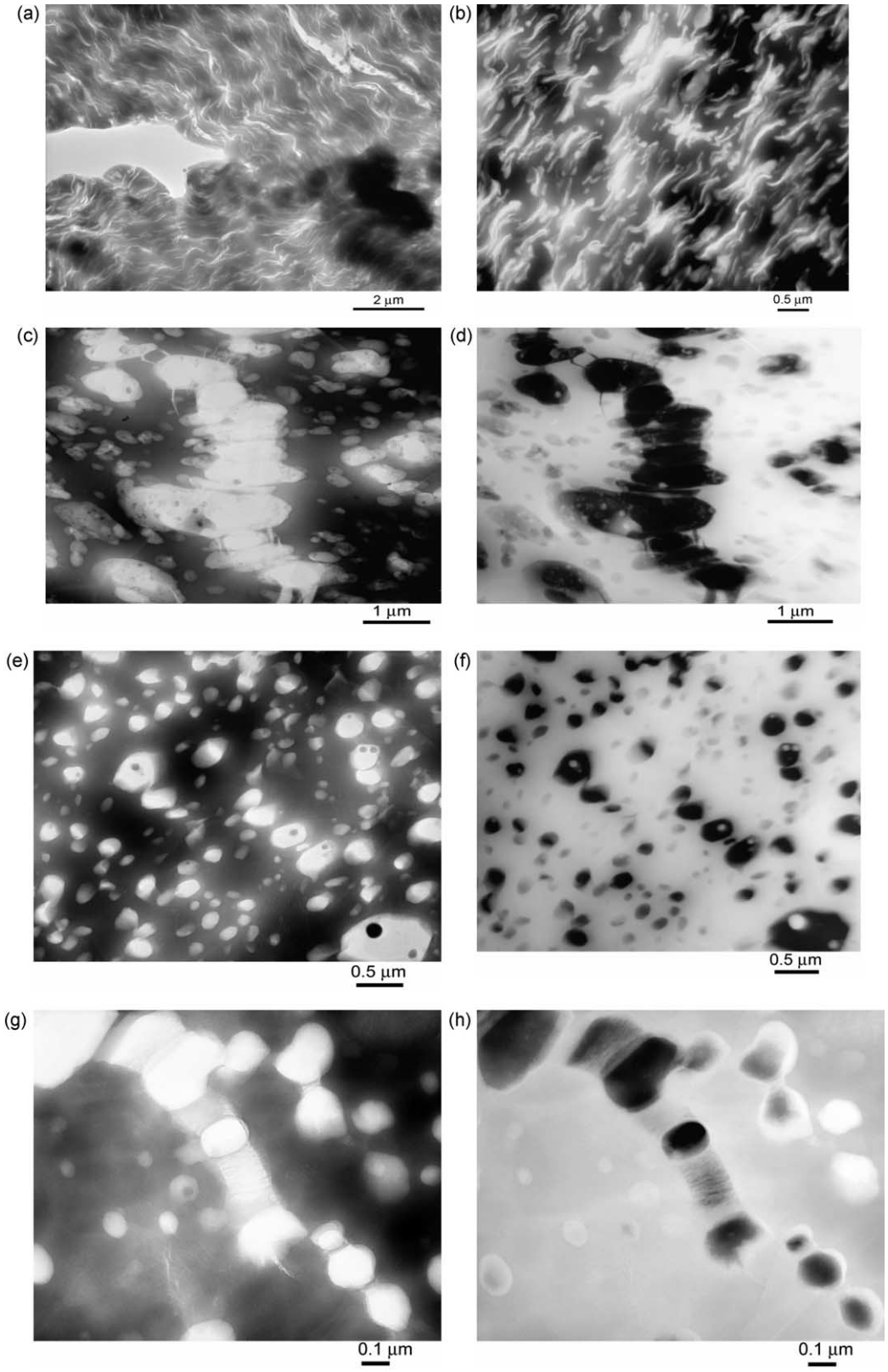

Fig. 16. TEM photomicrographs showing the morphology in the vicinity of an arrested crack tip in a 6.35 mm thick specimen with a sharp notch of a blend of nylon 6 containing 20 wt% of a mixture of EOR-*g*-MA-0.35%/EOR in a proportion of 40/60 in the rubber phase: (a) bright field image of the crack tip; (b) bright field image of about 30 μm ahead of the crack tip; (c) bright field image about 0.5 mm ahead of the crack tip but still inside the SWZ; (d) dark field image of (c); (e) bright field image about 1.1 mm ahead of the SWZ (about 2 mm away from the crack tip); (f) dark field image of (e); (g) bright field image from about the same position as (e); and (h) dark field image of (g).

7. Conclusions

The fracture behavior of an amorphous polyamide (designed as a-PA) and nylon 6 toughened with maleated ethylene/1-octene elastomers have been compared. The fracture behavior strongly depends on the blend composition, blend morphology (particle size and its distribution), sample geometry and test temperature for both systems. a-PA requires lower contents of rubber for super-toughness than nylon 6; blends of a-PA showed lower T_{db} and higher impact strength than nylon 6 blends at the same rubber content. Deformation mechanisms involved for a-PA and nylon 6 blends were observed to include cavitation of rubber particles followed by some crazing and then massive shear yielding of the matrix material.

The essential work of fracture analysis shows that, in general, at room temperature a-PA blends exhibit a greater non-essential work of fracture than nylon 6 blends, which is attributed to the larger size of the deformation zone around a crack; however, for the essential work of fracture, the opposite seems to be true. For certain blends of nylon 6, specimens from the far end from the gate of injection molded test bars showed a ductile–brittle transition at longer ligament lengths than did the gate end counterparts. For blends of nylon 6 exhibiting a bimodal size distribution, whether the failure is brittle or ductile depends on the average size of each population of particles rather than the global average. For both polyamides, the critical strain energy release rate, G_{IC}, increased with rubber content and temperature but decreased with rubber particle size.

Early studies demonstrated the role of rubber particle size on toughening of semi-ductile engineering polymers [70,71]. Wu proposed that the key parameter which determines whether the blend is ductile or brittle is a critical ligament thickness, i.e. surface to surface interparticle distance, rather than particle size itself [60]. The rational for this concept was based on the notion of percolation throughout the material of overlapping stress fields around the particles [71]. Despite the utility of the interparticle distance concept, it has been the object of some controversy [16,70,72]. More recently, Argon et al. used the interparticle distance point of view to explain toughening of semi-crystalline polymers in terms of a preferential crystalline layer of the matrix polyamide surrounding the particles [14,15]. It was proposed that the critical interparticle distance stems from percolation of the more ductile crystalline layers of the matrix through the entire structure. In this view, the toughening effect stems from a change in crystalline structure of the matrix around rubber particles caused by the presence of the particles. While clearly the crystalline morphology of the matrix should have some effect on mechanical behavior of the blend, the question addressed here is whether this is the central cause of a critical interparticle distance or particle size. The completely amorphous polyamide shows a critical rubber particle size for toughening at a fixed rubber content, and this size is nearly the same as that for semi-crystalline nylon 6. Thus, it seems apparent that this particle size effect must stem from a more general cause since it occurs in amorphous polyamides as well as semi-crystalline ones. Of course, there are significant differences in the toughening responses of a-PA and nylon 6 which may reflect the fact that one is semi-crystalline and the other is not; however, there are other differences between the two matrices that might be influential as well. Thus, it would be improper to attribute the fact that a-PA is toughened more easily than nylon 6 and that, in general, blends of a-PA have higher toughness than corresponding nylon 6 blends solely to the absence of crystallinity for a-PA or any particular crystalline morphology of nylon 6 blends.

Acknowledgements

The authors are grateful to PolyOne Distribution, Honeywell International Inc., and ExxonMobil Chemical Co. for providing the materials employed in this study.

References

[1] Huang JJ, Keskkula H, Paul DR. Polymer 2004;45:4203.
[2] Huang JJ, Keskkula H, Paul DR. Polymer 2006;47:639.
[3] Huang JJ, Keskkula H, Paul DR. Polymer 2006;47:624.
[4] Huang DD, Wood BA. Polym Prepr (Am Chem Soc, Div Polym Chem) 1992;33:629.
[5] Bucknall CB, Heather PS, Lazzeri A. J Mater Sci 1989;24:2255.
[6] Gaymans RJ, Borggreve RJM. Contemporary Top Polym Sci 1989;6:461.
[7] Sue HJ, Yee AF. J Mater Sci 1989;24:1447.
[8] Sue HJ, Yee AF. J Mater Sci 1991;26:3449.
[9] Lazzeri A, Bucknall CB. J Mater Sci 1993;28:6799.
[10] Bucknall CB, Karpodinis A, Zhang XC. J Mater Sci 1994;29:3377.
[11] Dijkstra K, Van Der Wal A, Gaymans RJ. J Mater Sci 1994;29:3489.
[12] Majumdar B, Keskkula H, Paul DR. J Polym Sci, Part B: Polym Phys 1994;32:2127.
[13] Janik H, Gaymans RJ, Dijkstra K. Polymer 1995;36:4203.
[14] Muratoglu OK, Argon AS, Cohen RE, Weinberg M. Polymer 1995;36:921.
[15] Argon AS, Bartczak Z, Cohen RE, Muratoglu OK. Novel mechanisms of toughening semi-crystalline polymers. In: Pearson RA, Sue HJ, Yee AF, editors. Toughening of plastics: advances in modeling and experiments. ACS symposium series, vol. 759. Washington, DC: American Chemical Society; 2000. p. 98.
[16] Bucknall CB. Deformation mechanisms in rubber-toughened polymers. In: Paul DR, Bucknall CB, editors. Polymer blends, 2nd ed, vol. 2. New York: Wiley; 2000. p. 83.
[17] Wong S-C, Mai Y-W. Polymer 2000;41:5471.
[18] Crouch BA, Huang DD. J Mater Sci 1994;29:861.
[19] Hashemi S, Williams JG. J Mater Sci 1991;26:621.
[20] Huang DD, Williams JG. J Mater Sci 1987;22:2503.
[21] Seidler S, Grellmann W. J Mater Sci 1993;28:4078.
[22] Zhou Z, Landes JD, Huang DD. Polym Eng Sci 1994;34:128.
[23] Williams JG. Fracture mechanics of polymers. New York: Halsted Press; 1984.
[24] Williams JG. ESIS Pulica 2001;28:3.
[25] Adams GC, Bender RG, Crouch BA, Williams JG. Polym Eng Sci 1990;30:241.
[26] Hashemi S, Williams JG. Polym Eng Sci 1986;26:760.
[27] Williams JG. Pure Appl Chem 1985;57:1679.
[28] Santana OO, Maspoch ML, Martinez AB. Polym Bull (Berlin) 1997;39:511.
[29] Standard test methods for plane-strain fracture toughness and strain energy release rate of plastic materials. D5045-99, ASTM; 1999.
[30] E-813 Standard test method for J_{IC}, a measure of fracture toughness, annual book of ASTM standards. ASTM: Philadelphia, PA; 1989.
[31] Mai YW, Cotterell B. Eng Fract Mech 1985;21:123.

[32] Mai YW, Cotterell B. Int J Fract 1986;32:105.
[33] Mai YW, Cotterell B, Horlyck R, Vigna G. Polym Eng Sci 1987;27:804.
[34] Kim JK, Mai YW. Compos Sci Technol 1991;41:333.
[35] Wu J, Mai Y-W. Polym Eng Sci 1996;36:2275.
[36] Mai YW, Wong SC, Chen XH. Application of fracture mechanics for characterization of toughness of polymer blends. In: Paul DR, Bucknall CB, editors. Polymer blends, 2nd ed, vol. 2. New York: Wiley; 1999 [chapter 20].
[37] Broberg KB. J Mech Phys Solids 1971;19:407.
[38] Broberg KB. J Mech Phys Solids 1975;23:215.
[39] Hale W, Keskkula H, Paul DR. Polymer 1999;40:3353.
[40] Okada O, Keskkula H, Paul DR. Polymer 2000;41:8061.
[41] Laura DM, Keskkula H, Barlow JW, Paul DR. Polymer 2001;42:6161.
[42] Pressly TG, Keskkula H, Paul DR. Polymer 2001;42:3043.
[43] Laura DM, Keskkula H, Barlow JW, Paul DR. Polymer 2003;44:3347.
[44] Kayano Y, Keskkula H, Paul DR. Polymer 1997;38:1885.
[45] Kayano Y, Keskkula H, Paul DR. Polymer 1998;39:2835.
[46] Wildes G, Keskkula H, Paul DR. Polymer 1999;40:7089.
[47] Majumdar B, Keskkula H, Paul DR. Polymer 1994;35:3164.
[48] Flexman EA. Polym Mater Sci Eng 1990;63:112.
[49] Bucknall CB. Toughened plastics. London: Applied Science Publishers Ltd; 1977.
[50] Williams DB, Carter CB. Transmission electron microscopy: a textbook for materials science. New York: Plenum Press; 1996.
[51] Lazzeri A, Bucknall CB. Polymer 1995;36:2895.
[52] Sue HJ. J Mater Sci 1992;27:3098.
[53] Sue HJ, Garcia-Meitin EI, Orchard NA. J Polym Sci, Part B: Polym Phys 1993;31:595.
[54] Sue HJ, Bertram JL, Garcia-Meitin EI, Puckett PM. J Polym Sci, Part B: Polym Phys 1995;33:2003.
[55] Paredes E, Fischer EW. Makromol Chem 1979;180:2707.
[56] Brown HR, Mills PJ, Kramer EJ. J Polym Sci, Polym Phys Ed 1985;23:1857.
[57] Bubeck RA, Buckley Jr DJ, Kramer EJ, Brown HR. J Mater Sci 1991;26:6249.
[58] Magalhaes AML, Borggreve RJM. Macromolecules 1995;28:5841.
[59] He C, Donald AM, Butler MF, Diat O. Polymer 1998;39:659.
[60] Wu S. J Appl Polym Sci 1988;35:549.
[61] Gaymans RJ. Toughened polyamides. In: Collyer AA, editor. Rubber toughened engineering plastics. London: Chapman & Hall; 1994. p. 210.
[62] Majumdar B, Keskkula H, Paul DR. J Appl Polym Sci 1994;54:339.
[63] Oshinski AJ, Keskkula H, Paul DR. Polymer 1996;37:4909.
[64] Majumdar B, Paul DR. Reactive compatibilization. In: Paul DR, Bucknall CB, editors. Polymer blends, 2nd ed, vol. 1. New York: Wiley; 2000. p. 539.
[65] Wu S. J Polym Sci, Polym Phys Ed 1983;21:699.
[66] Wu S. Polymer 1985;26:1855.
[67] Wu S. J Appl Polym Sci 1992;46:619.
[68] Epstein BN, Latham RA, Dunphy JF, Pagilagan RU. Elastomerics 1987;119:10.
[69] Ikeda RM. J Appl Polym Sci 1993;47:619.
[70] Borggreve RJM, Gaymans RJ, Schuijer J, Housz JFI. Polymer 1987;28:1489.
[71] Margolina A, Wu S. Polymer 1988;29:2170.
[72] Borggreve RJM, Gaymans RJ, Schuijer J. Polymer 1989;30:71.